

PROCEEDINGS OF SPIE

SPIDigitalLibrary.org/conference-proceedings-of-spie

Weighted least-squares image reconstruction in phase-contrast tomography

Pin-Yu Huang, Cheng-Ying Chou

Pin-Yu Huang, Cheng-Ying Chou, "Weighted least-squares image reconstruction in phase-contrast tomography," Proc. SPIE 7800, Image Reconstruction from Incomplete Data VI, 780008 (27 August 2010); doi: 10.1117/12.861062

SPIE.

Event: SPIE Optical Engineering + Applications, 2010, San Diego, California, United States

Weighted least-squares image reconstruction in phase-contrast tomography

Pin-Yu Huang^a and Cheng-Ying Chou^a

^aDepartment of Bio-Industrial Mechatronics Engineering
National Taiwan University, Taipei, Taiwan 106

ABSTRACT

X-ray phase-contrast tomography (PCT) methods seek to quantitatively reconstruct separate images that depict an object's absorption and refractive properties. Most PCT reconstruction algorithms generally operate by explicitly or implicitly performing the decoupling of the projected absorption and phase properties at each tomographic view angle by use of a phase-retrieval formula, followed by the inversion of X-ray transform. Tomographic reconstruction by use of statistical methods can account for the noise model and a priori information, and thereby can produce images with better quality over conventional filtered backprojection algorithms. We proposed a weighted least-squares method that takes into account the second-order statistical properties of the projected phase images and aims to minimize the objective function by employing a conjugate-gradient (CG) method. A computer-simulation study was carried out to investigate and evaluate the developed method.

Keywords: X-ray phase-contrast tomography, noise texture, weighted least-squares, conjugate-gradient

1. INTRODUCTION

X-ray phase-contrast imaging is a technique that can produce two separate images that respectively describe the phase and absorption properties of an object.¹⁻³ Because the contrast of phase property is several orders higher than that of absorption property, it can permit the visualization of the features with similar or identical absorption property. Additionally, phase contrast can persist at higher X-ray energies, and hence has the potential for low dose imaging. Provided its advantages over conventional X-ray methods, it is particularly suitable for biomedical imaging applications,⁴⁻⁶ and has been exploited to produce three-dimensional (3D) distribution^{1,7-9} of an object in phase-contrast tomography (PCT).

The tomographic reconstruction process can generally be divided into two steps. First, a phase retrieval formula is applied to yield a collection of projected phase and absorption estimates.¹⁰⁻¹² Subsequently, 3D distribution of refractive index can be reconstructed by inverting the X-ray transform. The phase retrieval formulas used to determine the complex amplitude contain the singularity that will result in greatly amplified low-frequency noise in the reconstructed images.

Recently, the analytic expression for image covariance in planar-mode phase-contrast imaging has been determined.¹³⁻¹⁵ The statistical properties of the projected estimates can be accounted for in the tomographic reconstruction to produce images with better quality over conventional filtered backprojection (FBP) algorithms. In this work, we employed a weighted least-squares method that takes into account the covariance properties of the projected phase images. The objective of the reconstruction method is to find an image that minimizes the cost function. This can be accomplished by employing the optimization algorithms such as conjugate-gradient method.¹⁶ A computer-simulation study was carried out to investigate and evaluate the developed method.

Further author information: Send correspondence to Cheng-Ying Chou, Ph.D.: E-mail: chengying@ntu.edu.tw

2. BACKGROUND

2.1 Imaging physics of In-line X-ray phase contrast tomography

In this section, we briefly review the imaging model of the in-line phase-contrast tomography developed by Cloetens.¹⁷ Consider a monochromatic wavefield U_i propagates along the z_r -axis and irradiates on the object centered at the origin of a reference coordinate system (x, y, z) . The object is characterized by its complex X-ray refractive index distribution as

$$n(\vec{r}) = 1 - \delta(\vec{r}) + i\beta(\vec{r}), \quad (1)$$

where $\vec{r} \equiv (x, y, z)$ and $i \equiv \sqrt{-1}$. The transmitted wavefield $U_t(x, y_r)$ on the contact plane immediately behind the object can be described by

$$U_t(x, y_r) = U_i \exp[-A(x, y_r) + i\phi(x, y_r)], \quad (2)$$

where the absorption and phase perturbations are respectively related to the complex refractive index as

$$A(x, y_r) = (2\pi/\lambda) \int \beta(\vec{r}) dz_r \quad (3)$$

and

$$\phi(x, y_r) = -(2\pi/\lambda) \int \delta(\vec{r}) dz_r. \quad (4)$$

The intensity of the transmitted wavefield is recorded on two or more detector planes at constant z_r , which are specified by the rotated coordinate (x, y_r) . The rotated coordinates (x, y_r, z_r) are related to the reference system as $y_r = y \cos \theta + z \sin \theta$ and $z_r = -y \sin \theta + z \cos \theta$. On the detector plane $z_r = z_d$ behind the object, the measured intensity is related to the transmitted wavefield as

$$I_d(x, y_r) = |U_t(x, y_r) * h_{z_d}(x, y_r)|^2, \quad (5)$$

where the $h_{z_d}(x, y_r)$ is Fresnel propagator and ‘**’ denotes the two-dimensional convolution operation. The tomographic scanning is performed by keeping the object fixed while simultaneously rotating the X-ray source and the detector, or equivalently, by keeping the imaging system fixed and rotating the object. A schematic of the scanning geometry for PCT is illustrated in Fig. 1. For simplicity, the tomographic view angle θ will be suppressed in the equations below.

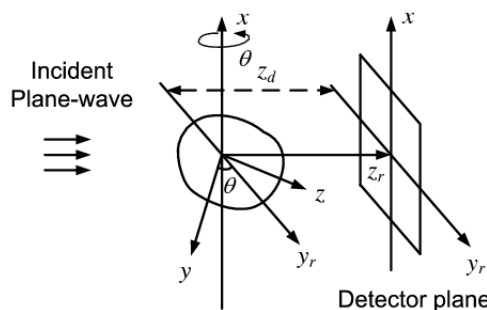


Figure 1. A schematic of the scanning geometry of in-line phase-contrast tomography.

2.2 Image reconstruction

Assuming that $|A(x, y_r)| \ll 1$ and $\phi(x, y_r)$ is varying smoothly,¹⁸⁻²⁰ it has been demonstrated that $A(x, y_r)$ and $\phi(x, y_r)$ can be determined readily by the algebraic formulas in Fourier domain as

$$\tilde{A}_{m,n}(u, v_r) = \frac{\sin(\pi\lambda z_n f^2) \tilde{I}_m(u, v_r) - \sin(\pi\lambda z_m f^2) \tilde{I}_n(u, v_r)}{2 \sin[\pi\lambda f^2(z_m - z_n)]} \quad (6)$$

and

$$\tilde{\phi}_{m,n}(u, v_r) = \frac{\cos(\pi\lambda z_n f^2)\tilde{I}_m(u, v_r) - \cos(\pi\lambda z_m f^2)\tilde{I}_n(u, v_r)}{2 \sin[\pi\lambda f^2(z_m - z_n)]}, \quad (7)$$

respectively,^{17,21} where $f^2 \equiv u^2 + v_r^2$ and the subscripts m, n have been added to $\tilde{A}(u, v_r)$ and $\tilde{\phi}(u, v_r)$ to denote that they are estimated by use of measurements $I_m(x, y_r)$ and $I_n(x, y_r)$. Note that a singularity is present at the zero frequency $u = v_r = 0$ in Eq. (7), indicating that the low-frequency components of $\phi(x, y_r)$ will contain greatly amplified noise levels. The pole will affect the noise properties of the reconstructed phase image $\phi(x, y_r)$ and $\delta(x, y, z)$.

The tomographic reconstruction problem can be approximated by the discrete linear model

$$\vec{g} = \mathcal{H}\vec{f}, \quad (8)$$

where $\vec{g} \in \mathbb{R}^M$ corresponds to projection measurements, $\vec{f} \in \mathbb{R}^N$ denotes the object function, and $\mathcal{H} \in \mathbb{R}^{M \times N}$ denotes the discrete approximation of X-ray transform. The application of inverse Fourier transform to Eqs. (6) and (7) allows for estimation of $A(x, y_r)$ and $\phi(x, y_r)$ at each view angle. Subsequently, $\beta(x, y, z)$ and $\delta(x, y, z)$ can be obtained by inverting the X-ray transform. This can be accomplished by applying a statistical reconstruction method that aims to find the solution that minimizes the mismatch between the observed data and the reconstructed image. A penalized weighted least-squares method that takes into consideration of the statistical properties of the observed data is a useful approach to obtain the solution. The cost function $\Phi(\vec{f})$ that we aim to minimize take on the following form,¹⁶

$$\Phi(\vec{f}) = \frac{1}{2}(\vec{g} - \mathcal{H}\vec{f})^T W(\vec{g} - \mathcal{H}\vec{f}) + \eta R(\vec{f}), \quad (9)$$

where $R(\vec{f})$ is the penalty function, which smoothes the the object function \vec{f} , η is the regularized parameter that controls the tradeoff between the noise and resolution, and W corresponds to the inverse of covariance matrix of \vec{g} . This will yield an estimate of \hat{f} that satisfies

$$\hat{f} = \arg \min_{\vec{f}} \Phi(\vec{f}). \quad (10)$$

In phase-contrast tomography, \vec{g} is the estimated $A_{m,n}(x, y_r)$ or $\phi_{m,n}(x, y_r)$, and \vec{f} refers to the corresponding $\beta_{m,n}(\vec{r})$ or $\delta_{m,n}(\vec{r})$.

3. NOISE MODEL

In the presence of stochastic noise, the measured intensity will be denoted as $\mathbf{I}_m(x, y_r)$, where hereafter boldface and normal fonts will denote a stochastic quantity and its mean, respectively. We consider a measurement model²²

$$\mathbf{I}_m(x, y_r) = I_m(x, y_r) + \mathbf{n}(x, y_r), \quad (11)$$

where $\mathbf{n}(x, y_r)$ denotes an additive noise term. We assume the noise satisfies

$$\text{Cov}\{\mathbf{n}_m(x, y_r), \mathbf{n}_{m'}(x', y'_r)\} = \text{Var}\{\mathbf{n}_m(x, y_r)\}\delta(x - x')\delta(y - y'_r)\delta_{mm'}, \quad (12)$$

where $\text{Cov}\{\mathbf{n}_m(x, y_r), \mathbf{n}_{m'}(x', y'_r)\}$ and $\text{Var}\{\mathbf{n}_m(x, y_r)\}$ denote covariance and variance of the noise.

4. NUMERICAL RESULTS

Computer simulation studies were conducted to investigate the effect of covariance matrix on the statistical properties of reconstructed images in PCT.

4.1 Numerical phantom and image reconstruction

A mathematical phantom comprised of 4 uniform ellipsoids was employed to represent the object. The wavelength of the incident monochromatic X-ray beam was 0.8265 \AA . The intensity data were acquired on two distinct detector planes positioned at 100 and 230 mm behind the object, respectively. The detector was assumed to contain 128×128 elements of dimension of $5 \text{ }\mu\text{m}$. Noisy intensity data were produced according to Eq. (11), where the standard deviation of Gaussian noise was $\sigma=1\%$. Estimates of the Fourier components of $\tilde{A}(u, v_r)$ and $\tilde{\phi}(u, v_r)$ were reconstructed by use of Eqs. (6) and (7), respectively. From these Fourier data, estimates of $A(x, y_r)$ and $\phi(x, y_r)$ were obtained after the application of the 2D inverse Fourier transform. A set of tomographic data were obtained by repeating the above procedures at 180 equally distributed tomographic view angles θ over $[0, 180^\circ)$.

The covariance properties of the projected estimates were computed analytically by use of Eqs. (31) and (33) in Ref.¹⁴. The elements of the weighting matrix W in Eq. (9) were specified by inverting the computed covariance matrix. In order to search for the solution that minimizes the objective function expressed in Eq. (9), the conjugated gradient method was employed. In this work, we used the Polak-Ribiere CG method to calculate the search direction solve the inverse problem iteratively, and the regularized parameter was set at $\eta = 0.01$.^{16,23}

4.2 Numerical results

An example of noisy reconstructed images of $A(x, y_r)$ and $\phi(x, y_r)$ is contained in Fig. 2. It can be seen that $\phi(x, y_r)$ is contaminated by low frequency noise, while $A(x, y_r)$ is not. This is consistent with the prediction made in the previous noise analysis.¹⁴ Although the ramp filter in the classical FBP algorithm can help to mitigate the Fourier pole at the zero-frequency, the reconstructed tomographic refractive index images still possess high low-frequency noise, as compared to the attenuation images.²⁴

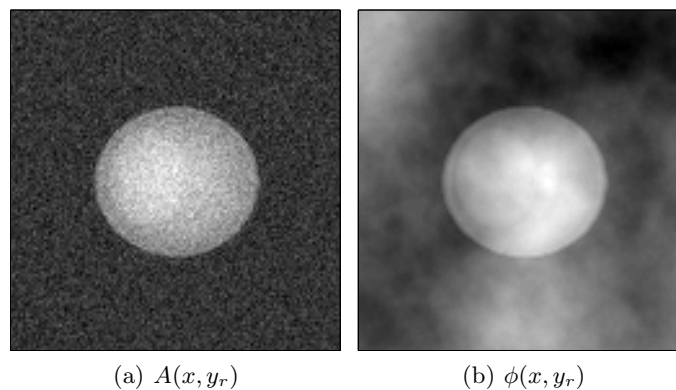


Figure 2. Estimates of (a) $A(x, y_r)$ and (b) $\phi(x, y_r)$ reconstructed from noisy data for imaging geometry with detector spacing $\Delta z = 130 \text{ mm}$

Next, the collection of phase estimates was used as the projection data for tomographic reconstruction. This was accomplished by use of FBP and the penalized weighted least-squares algorithms, respectively. The reconstructed estimates of $\delta(\vec{r})$ corresponding to the transverse slice $x = 0$ are presented in Fig. 3, in which the subfigures (a) and (b) correspond to the images reconstructed by use of the FBP and the penalized weighted least-squares algorithms, respectively. The images contained in Fig. 3 appear to possess different noise textures, as the applied algorithms differ.

The statistical properties of phase-contrast tomography using the FBP and weighted least-squares methods were computed from ensembles of 1000 and 180 noisy realizations of intensity measurement pairs $\mathbf{I}_1(x, y_r)$ and $\mathbf{I}_2(x, y_r)$. The covariance properties of the refractive images obtained by use of FBP and the weighted least-squares methods are contained in Figs. 4(a) and (b). In contrast to the corresponding FBP result, both the magnitude of the covariance of $\delta(\vec{r})$ and the degree of noise correlation for the weighted least-squares one are reduced.

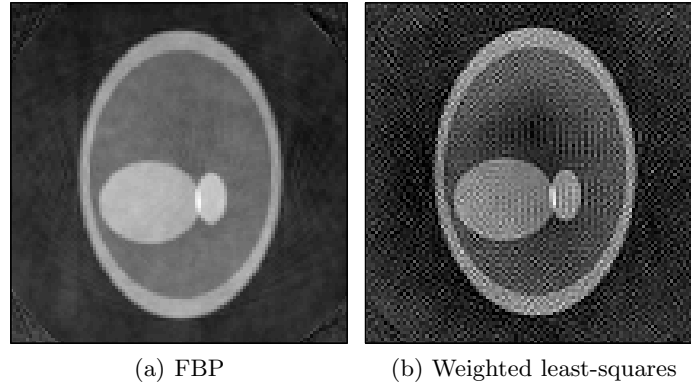


Figure 3. Estimates of $\delta(0, y, z)$ reconstructed by use of the (a) FBP and (b) penalized weighted least-squares algorithms at the 64th iteration.

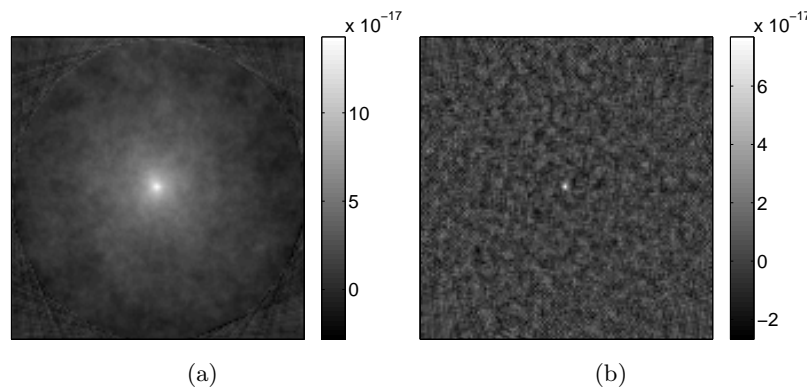


Figure 4. The covariance maps $\text{Cov}\{\delta(0, y, z), \delta(0, 0, 0)\}$ of the images reconstructed by use of the (a) FBP and (b) penalized weighted least-squares algorithms.

5. SUMMARY

In this work, we investigated the statistical properties of the reconstructed images in X-ray phase-contrast tomography. We employed the penalized weighted least-squares method and utilized the analytically computed covariance of the projected phase as *a priori* information in PCT reconstruction. The estimates of the covariance properties of the 3D real-valued refractive index distributions resulted from the FBP and the proposed algorithms were determined empirically. We observed that the values of covariance properties of the reconstructed refractive index are mitigated by taking the noise properties of data functions into consideration during the reconstruction process. It was also found that the degree of the correlation in the reconstructed phase images is reduced.

ACKNOWLEDGMENTS

This work was supported in part by National Science Council under grant No. NSC 99-2221-E-002-043-MY3.

REFERENCES

1. Cloetens, P., Ludwig, W., Boller, E., Helfen, L., Salvo, L., Mache, R., and Schlenker, M., “Quantitative phase-contrast tomography using coherent synchrotron radiation,” in [*Developments in X-ray Tomography III, Proceedings of the SPIE*], **4503**, 82–91 (2002).
2. Mayo, S., Davis, T., Gureyev, T., Miller, P., Paganin, D., Pogany, A., Stevenson, A., and Wilkins, S., “X-ray phase-contrast microscopy and microtomography,” *Optics Express* **11**(19), 2289 – 2302 (2003).
3. Paganin, D. M., [*Coherent X-Ray Optics*], Oxford University Press, New York (2006).

4. Lewis, R. A., "Medical phase contrast x-ray imaging: current status and future prospects," *Physics in Medicine and Biology* **49**(16), 3573–3583 (2004).
5. Fiedler, S., Bravin, A., Keyrilainen, J., Fernandez, M., Suortti, P., Thomlinson, W., Tenhenun, M., Virkkunen, P., and Karjalainen-Lindsberg, M., "Imaging lobular breast carcinoma: comparison of synchrotron radiation CT-DEI technique with clinical CT, mammography and histology," *Physics in Medicine and Biology* **49**, 1–15 (2004).
6. Arfelli, F., Bonvicini, V., Bravin, A., Cantatore, G., Castelli, E., Palma, L. D., Michiel, M. D., Fabrizioli, M., Longo, R., Menk, R. H., Olivo, A., Pani, S., Pontoni, D., Poropat, P., Prest, M., Rashevsky, A., Ratti, M., Rigon, L., Tromba, G., Vacchi, A., Vallazza, E., and Zanconati, F., "Mammography with synchrotron radiation: Phase-detection techniques," *Radiology* **215**, 286–293 (2000).
7. Bronnikov, A. V., "Theory of quantitative phase-contrast computed tomography," *Journal of the Optical Society of America A* **19**(3), 472 – 480 (2002).
8. Gureyev, T. E., Nesterets, Y. I., Paganin, D. M., and Wilkins, S. W., "Effects of incident illumination on in-line phase-contrast imaging," *J. Opt. Soc. Am. A* **23**(1), 34–42 (2006).
9. McMahon, P., Peele, A., Paterson, D., Nugent, K. A., Snigirev, A., Weitkamp, T., and Rau, C., "X-ray tomographic imaging of the complex refractive index," *Appl. Phys. Lett.* **83**, 1480–1482 (2003).
10. Nugent, K. A., Gureyev, T. E., Cookson, D. F., Paganin, D. M., and Barnea, Z., "Quantitative phase imaging using hard x-rays," *Physical Review Letters* **77**, 2961–2964 (1996).
11. Cloetens, P., Pateyron-Salome, M., Buffiere, J. Y., Peix, G., Baruchel, J., Peyrin, F., and Schlenker, M., "Observation of microstructure and damage in materials by phase sensitive radiography and tomography," *Journal of Applied Physics* **81**, 5878–5886 (1997).
12. Langer, M., Cloetens, P., Guigay, J. P., and Peyrin, F., "Quantitative comparison of direct phase retrieval algorithms in in-line phase tomography," *Med Phys* **35**(10), 4556–66 (2008).
13. Chou, C.-Y. and Anastasio, M. A., "Influence of imaging geometry on noise texture in x-ray in-line phase-contrast imaging," in [*Proceedings of the SPIE*], Hsieh, J. and Samei, E., eds., *Medical Imaging 2008: Physics of Medical Imaging* **6913**(1), 69131Z (2008).
14. Chou, C.-Y. and Anastasio, M. A., "Influence of imaging geometry on noise texture in quantitative in-line x-ray phase-contrast imaging," *Optics Express* **17**(17), 14466–14480 (2009).
15. Chou, C.-Y. and Anastasio, M. A., "Statistical properties of x-ray phase-contrast tomography," in [*Annual International Conference of the IEEE Engineering in Medicine and Biology Society, 2009. EMBC 2009*], 6648 –6650 (2009).
16. Fessler, J. and Booth, S., "Conjugate-gradient preconditioning methods for shift-variant PET image reconstruction," *IEEE Transactions on Image Processing* **8**(5), 688–699 (1999).
17. Cloetens, P., *Contribution to Phase Contrast Imaging, Reconstruction and Tomography with Hard Synchrotron Radiation: Principles, Implementation and Applications*, PhD thesis, Vrije Universiteit Brussel (1999).
18. Guigay, J.-P., "Fourier transform analysis of Fresnel diffraction patterns and in-line holograms," *Optik* **49**, 121–125 (1977).
19. Wu, X. and Liu, H., "Clinical implementation of x-ray phase-contrast imaging: Theoretical foundations and design considerations," *Medical Physics* **30**, 2169–2179 (2003).
20. Kotre, C. J. and Birch, I. P., "Phase contrast enhancement of x-ray mammography: a design study," *Physics in Medicine and Biology* **44**, 2853–2866 (1999).
21. Cloetens, P., Ludwig, W., Boller, E., Helfen, L., Salvo, L., Mache, R., and Schlenker, M., "Quantitative phase contrast tomography using coherent synchrotron radiation," *Proceedings of SPIE - The International Society for Optical Engineering* **4503**, 82–91 (2001).
22. Paganin, D., Barty, A., McMahon, P. J., and Nugent, K. A., "Quantitative phase-amplitude microscopy III. The effects of noise," *Journal of Microscopy* **214**, 51–61 (2003).
23. Mumcuoglu, E., Leahy, R., Cherry, S. R., and Zhou, Z., "Fast gradient-based methods for Bayesian reconstruction of transmission and emission PET images," *IEEE transactions on Medical Imaging* **13**(4), 687–701 (1994).
24. Chou, C.-Y. and Anastasio, M. A., "Noise texture and signal detectability in propagation-based x-ray phase-contrast tomography," *Medical physics* **37**, 270 (2010).